Control of a three-dimensional blunt body wake using low and high frequency pulsed jets

D. Barros*[1,2], T. Ruiz[2], J. Borée[1], and B.R. Noack[1]
[1]Institut Pprime, UPR-3346 CNRS, ISAE-ENSMA, Université de Poitiers, Futuroscope Chasseneuil, France.
[2]PSA Peugeot Citroën, Centre Technique de Vélizy, 78943, Vélizy-Villacoublay Cedex, France

Abstract
We present experimental evidence of pressure changes in the wake of a three-dimensional blunt body by the use of periodic pulsed jets. The jets are pulsed tangentially to the shear layers separated from the trailing-edges of a classical square-back Ahmed body. The Reynolds number based on the model's height is $Re_H = 3.10^5$. Significant decrease (respectively increase) of the rear pressure are achieved considering low and high frequency pulsing. Low frequency actuation ($St = Hf/U_o = 0.4$, where f is the frequency and U_o the upstream velocity) is shown to enhance the global wake mode and to increase drag. On the contrary, dynamical effects associated to the particular flow control strategy provides a significant drag decrease for the higher frequency forcing ($St = 11.5$). Time-averaged pressure on the back surface of the model and velocity measurements on the wake illustrates the main effects of such actuation and introduce new strategies for drag control of three-dimensional geometries.

1. INTRODUCTION

Controlling the flow around complex geometries for drag reduction has been a challenging and multi-disciplinary field in flow control research. The flow around bluff bodies and the associated drag has extensively been discussed in important studies as the seminal works of Roshko[1][2], and particularly in the road vehicles aerodynamics as described in [3] and [4]. This subject inspired numerous projects to achieve a better understanding of the flow physics and the guidelines to perform successful control strategies, both of them were recently reviewed in [5].

Several spatial and temporal dynamics characterize the flow mechanisms around bluff bodies. Generally, boundary layers separate in the rear part of the model creating a large region of recirculating flow. When this separation is set by geometric constraints, the model is then commonly referred to blunt body.

In nominally two-dimensional geometries, as the case of blunt-trailing edge cylinders, the Kármán vortex shedding is developed just after flow separation, inducing periodic motion in the near wake and considerable pressure drag. Drag control of these flows has largely been studied by different ways [6][7][8][9]. They investigated how steady and unsteady perturbations modify the mechanism of alternating vortex shedding, resulting in significant modifications of drag.

Three-dimensional blunt geometries were also subject of flow control strategies for drag reduction, some of them with significant results as described by [10],[11], [12], [13] and [14]. The flow around them is considerably different from the two-dimensional analogues. Here, the recirculation region is also formed but the strong alternate shedding is not observed anymore. The dynamical flow mechanisms seem to be mainly governed by the development of the shear-layers separated from the trailing-edges in addition to the appearance of global shedding at the end of the recirculation region. Besides, long-time dynamics corresponding to random changes of flow topology are also found in this flow, as recently observed by [15].

*diogo.barros@ensma.fr

An important parameter for the wake control is the choice of actuation: how is it possible to perform a successful control of the flow around a three-dimensional geometry without changing its geometric properties? Is the best control strategy unsteady or simply a steady perturbation? The use of pulsed jets in specific points of the model's surface seems to be an interesting alternative as it does not alter the complex geometry of the model. Besides, its use allows great flexibility for the interactions with the flow unsteadiness being then a nice candidate for real-time closed loop control plants. Some studies showed the use of pulsed jets in other three-dimensional models for flow control as exemplified by [16] and [17].

The present study attests the capability of periodic pulsed jets [18] as a geometry-free flow control strategy in order to alter the wake dynamics and change the pressure distribution of the rear part of a blunt-trailing edge model. Pressure changes in this region are intimately related to drag and correspond to almost 70% of the total drag of some models [19]. Its control is then a direct way to reduce the pressure drag. Pressure measurements on the rear surface of the body as well as velocity fields in the wake are analyzed to draw a picture of the main modifications of such kind of control that affects directly and dynamically the turbulent near wake.

The work is presented as follows: the experimental set-up is described in section 2: the model and wind tunnel characteristics are highlighted as well as the measurement apparatus and control description. We illustrate in section 3 the effect of periodic forcing on the rear-pressure of the model, and the main changes in the wake velocities: both time-averaged and velocity fluctuations are considered. We also propose in section 3 physical mechanisms responsible for the noticeable drag reduction observed. Finally, a dynamical description of the wake is discussed based on flow snapshots and on the spectral content of the near wake.

2. EXPERIMENTAL SET-UP

2.1 Model description and wind tunnel

The three-dimensional blunt body studied here is a similar geometry of the so-called square back Ahmed model found in [3]. Flow dynamics around this model shares many similarities with the aerodynamics of real road vehicles. The model has an overall length $L = 0.893m$, a width $W = 0.350m$ and a height $H = 0.297m$. It is mounted over a NACA-profiled leading-edge flat plate in order to control the incoming boundary layer. The connection of the model and the flat plate is done by the use of four profiled supports with a ground clearance of $G = 0.05m$. Figures 1(a,b) illustrate a scheme of the general configuration and its respective dimensions. The origin of the reference system (O) is placed conveniently on the symmetry plane of the configuration over the floor (see figure 1a).

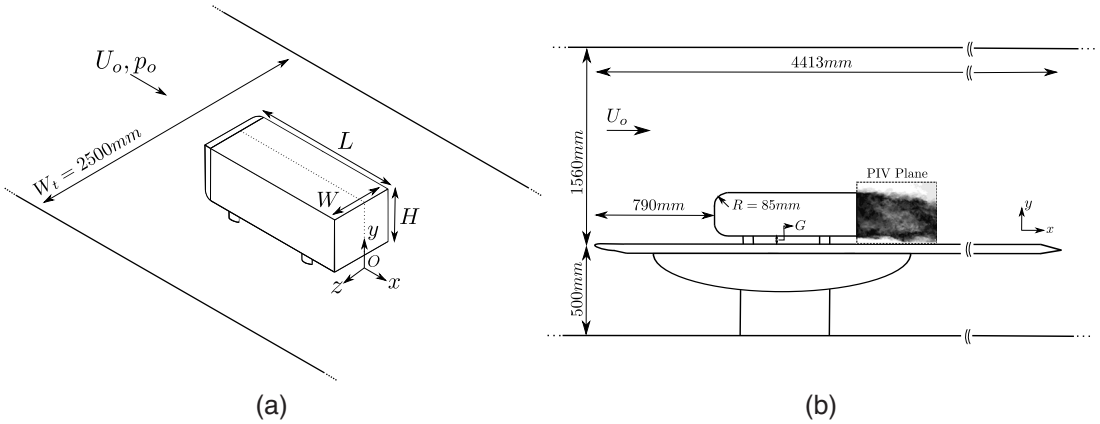

(a) (b)

Figure 1. Geometric description of the configuration. a) Ahmed body mounted on the floor in a 3D view. b) Lateral view of the wind tunnel test section. The origin of the coordinate system is indicated by O and placed over the floor on the symmetry plane of the configuration.

The experiments were performed in the PSA-Peugeot Citröen wind tunnel described in details by [20]. Wind tunnel velocities can be varied from 5m/s to 50m/s and here the upstream velocity is kept constant and equal to $U_o = 15m/s$. The Reynolds number based on the height of the model is $Re_H = 3.10^5$. Considering the boundary layer at separation on the upper shear layer of the model ($x/H = 0$ and $y/H = 1.16$), the 99% boundary layer thickness and the momentum deficit thickness are respectively $\delta_{99\%}/H = 0.135$ and $\theta/H = 0.0124$ with a shape factor of 1.21. We define the streamwise, wall-normal and transverse velocities by u, v and w corresponding respectively to the x, y and z axes.

2.2 Pressure and velocity measurements

In order to detect drag variations corresponding to rear pressure changes when control is applied, 17 pressure taps were installed at the back surface of the model to quantify the overall base pressure distribution. Pressure measurements were obtained using a 64-port HD miniature scanner with an SCANdaq 8.000 interface and each pressure value is time-averaged over $45s$ (which corresponds approximately to 2273 convective time units H/U_o).

Near wake velocity was measured using particle image velocimetry (PIV) and hot wire anemometry (HWA). The PIV system is able to measure two components of the velocity field in the symmetry plane of the Ahmed model ($z = 0$) as well as in a transverse (horizontal) plane at mid-height of the body ($y/H = 0.67$). The laser sheet is created by a Quantal Big Sky Laser (dual pulse Nd:YAG) and two DANTEC CCD cameras (FlowSense MkII, 4Mpx) were used in parallel to obtain a global view of the wake. A laser sheet was pulsed (with time delays of $120\mu s$) and acquisitions were made with a sampling frequency of 4Hz, for which ensembles of 1000-2000 images pairs were used to obtain the time-averaged flow and second-order statistics. Velocity vectors calculations are processed with an interrogation window of 32x32 pixels (an overlap of 50%) giving a spatial resolution of 1% of the model's height. Considering an absolute displacement error of 0.1 pixels, the maximum uncertainty on instantaneous velocity fields are estimated to be 0.2 m/s. Statistical errors are estimated based on 1000-2000 velocity fields to be about $0.05u_{rms}$ (root mean square value of the velocity field in a point).

Hot wire measurements using a single wire probe (55P11) were acquired by a StreamlinePro Anemometer System (from Dantec Dynamics®) in order to evaluate the unsteady and the spectral behavior of the wake as well as to calibrate the pulsed jets used for control, as described in the next section. The probe was mounted inside a 55H21 support. The calibration of the constant temperature anemometer (CTA) system was performed by an automatic calibrator of the same manufacturer. The measurements were sampled at a frequency of 2.5KHz and the duration of each test was 120s.

2.3 Control parameters

Pulsed jets are characterized by different parameters like the exit velocity, the thickness of the plane jet, the direction of blowing and its frequency. In this work we will focus on the frequency effects of plane pulsed jets for a given amplitude. Figure 2 illustrates a scheme of the main control parameters and its detailed design. The generation of a jet with specified velocity V_j depends on the pressure difference between the input pressure P_i in the compressed air cylindrical reservoir and the outside pressure. The input pressure can be adjusted to values up to 5 bars. The compressed air is then distributed to an ensemble of 32 solenoid valves homogeneously separated along the four trailing edges of the body, in order to improve spatial homogeneity of the pulsed flow. Air passes through an elbowed duct (described in the Exit Zone detail) until arriving at the exit slit section of thickness h=(1±0.1) mm, where the jet is pulsed tangentially to the upper surface of the model (and then tangentially to the upstream flow corresponding to the separating shear layers). The pneumatic solenoid valves used here (Matrix OX 821.100C2KK series) can be individually commanded by rectangular waveform signals and their frequencies can be varied from 0 Hz (steady blowing) to about 600 Hz.

To simplify the number of parameters, we have considered the same frequency (called hereafter F_i) all along the four trailing edges and a fixed pressure input P_i of 1.45 bar. Without loss of generality, the duty cycle (DC) of the signals was settled as 40%. The characteristics of the plane pulsed jets were carefully measured using a specific test rig outside the wind tunnel. Due to the imperfections of the mounting ducts inside the body and their complex geometry, the time-averaged slit centerline velocity V_{jmax} can have variations of at most ±10% along the four trailing edges.

We consider dimensionless frequencies based on the model's geometry (H) and on the boundary layer momentum thickness (θ), respectively defined as $St_H = F_iH/U_o$ and $St_\theta = F_i\theta/(U_o/2)$. Two actuation frequencies are studied in the present work: $St_H = 0.4$ ($St_\theta = 0.0098$) and $St_H = 11.5$ ($St_\theta =$

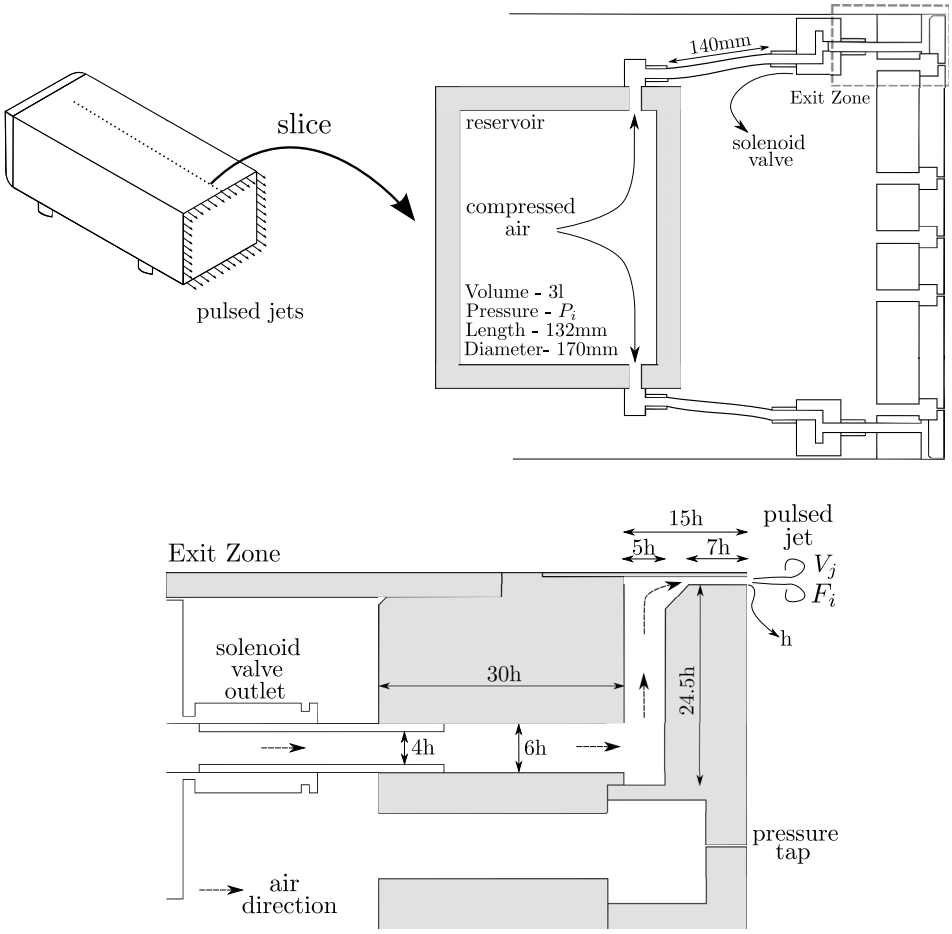

Figure 2. Scheme of the main control design and parameters. Two inputs are considered: P_i (pressure in the compressed air reservoir) and F_i (input frequency in the solenoid valves). A slice in the symmetry plane of the configuration is done in order to better describe the reservoir and the air path inside the ducts. Until the exit slit the air passes through an elbowed duct which is detailed in the Exit Zone (lower figure). The final pulsed jets have an exit velocity V_j and a frequency F_i.

0.284), respectively designated, for the sake of simplicity, low-frequency (LF) and high-frequency (HF) actuation. These frequencies were selected for a detailed analysis because they have important consequences on the pressure drag value. They represent completely different time scales considering the natural wake frequencies commonly found in the literature. Shedding of vortices has been observed in similar geometries [11] [15] [25] at Strouhal numbers (St_H) of the order of 0.17-0.2, corresponding approximately to the half of the first chosen actuation frequency. On the other hand, $St_\theta = 0.284$ is considerably greater than all of typical frequencies observed in the shear layers developed from the separated flow in the trailing edges, at least when one takes into account the most amplified frequencies in plane shear layers, namely $St_\theta = 0.044 - 0.048$ for turbulent shear layers [21]. Table 1 summarizes the dimensionless actuation frequencies and the commonly observed natural wake modes in the Ahmed body wake.

Jet velocity was characterized for the two aforementioned frequencies. Measurements were performed using a single-probe hot wire. Figure 3a illustrates the time evolution of the centerline velocity at 1 *mm* downstream the slit exit cross-section. First, the different behavior of the two velocity waveforms is noticeable: HF actuation behaves more like triangular waves contrary to the typical rectangular signal observed in the LF actuation. Besides, differences in the peak velocity were also remarked: the peak velocities observed in the LF case are constant for many cycles while low amplitude modulation is observed for HF configuration. We perform a phase average of these signals to evaluate the typical waveform during one period. Figure 3b shows the phase averaged mean velocity for both

actuation. Clearly the maximum mean velocity of HF actuation is smaller than the LF case. For a phase angle $\phi = \pi$, the standard deviation of the phase average velocity is about 2 m/s for both configurations. In addition, the rectangular wave behavior is again observed for the LF actuation contrary to the HF configuration where a sinus-like waveform is obtained in the phase averaged signal. Finally, the spectral content of both signals is analyzed by the power spectral density (PSD) of the velocities, presented in figure 3c. We can note the first high-amplitude peak corresponding to the actuation frequency ($f/F_i = 1$) and its expected harmonics.

Table 1. Dimensionless actuation frequencies and main natural wake modes commonly observed in the Ahmed body wake.

Configuration	St_H	St_θ
Natural flow: global shedding	0.17-0.2*	0.004-0.005
Natural flow: shear layers	1.78-1.94	0.044-0.048**
LF actuation	0.4	0.0098
HF actuation	11.5	0.284

* after [11], [15] and [25]; ** from [21].

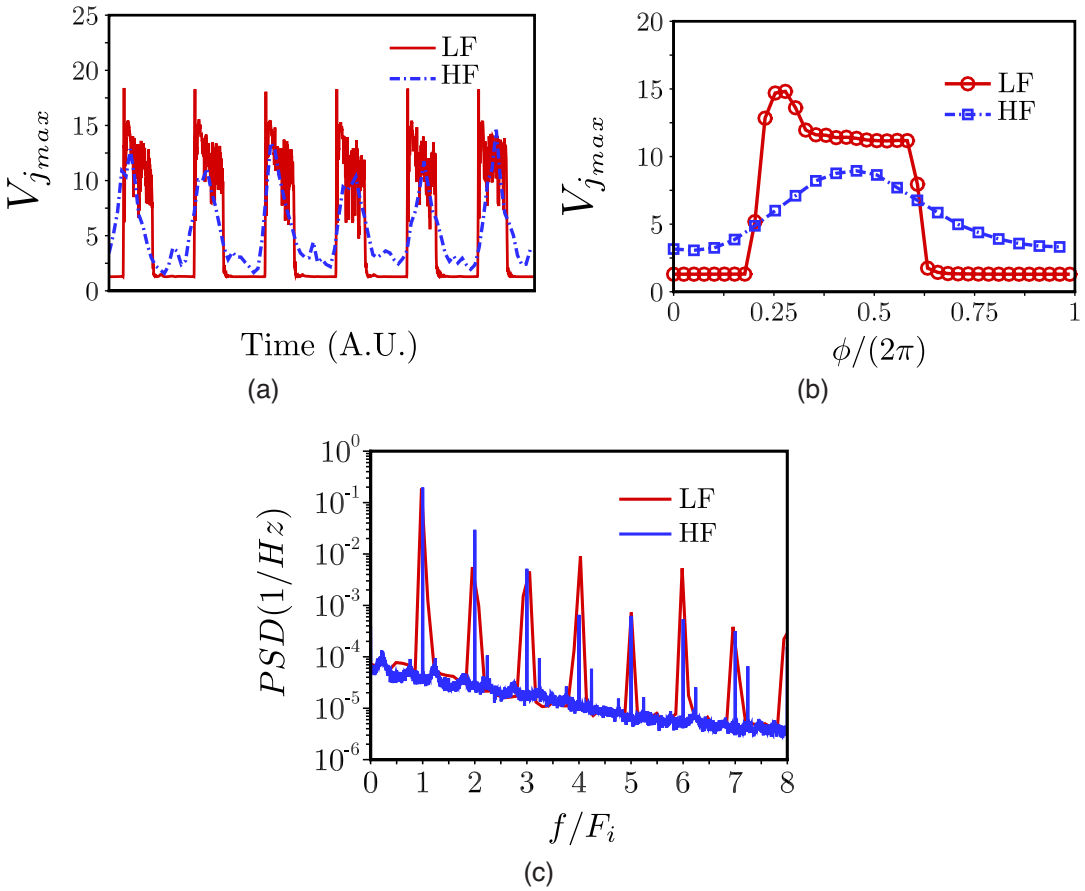

Figure 3. Hot wire measurements of the pulsed jet 1 mm downstream its exit section. a) Time evolution of the velocity in the center of the jet (V_{jmax} in m/s). b) Phase averaged mean velocity. c) PSD of the pulsed jets.

3. RESULTS AND DISCUSSION

3.1 Effects of control on the rear pressure

Control effects on the base pressure of the model are discussed in this section. Figure 4(a,b,c) presents the pressure coefficient $C_p = (p - p_o)/(\rho U_o^2/2)$ distribution in the back of the Ahmed body for the natural and controlled flows. Noticeably, the periodic control promotes a significant modification of the back pressure. Actuation with the lower frequency is responsible for a considerable decrease of the spatially averaged pressure coefficient of about 18%. On the other hand, higher frequency actuation is capable of increasing back pressure by almost 10%, reducing then the pressure drag of the body (this corresponds to an estimated 7% of drag reduction based on [19]). For comparison, continuous blowing was tested using the same input pressure (not discussed here for brevity) and it was responsible for a slight increase of the spatially averaged back pressure (about 2%).

By comparing figures 4(a,c), a noticeable mean pressure increase is observed in the upper region of the base of the model for the higher actuation frequency. More quantitatively, if δC_p is the difference of the pressure coefficient between the upper and lower region of the base, $\delta C_p = 0.021$ for the upper part and $\delta C_p = 0.014$ for the lower part indicating then an increase of base pressure of about 50% greater on the upper portion of the model's base.

In order to quantify control efficiency for the high frequency actuation case, we define (see [13]) the efficiency parameter ζ as the ratio of the power saved due to the drag reduction ($P_s = |\Delta C_x|(\rho U_o^3/2)A$, where A is the frontal area of the model and C_x the model's drag coefficient) and the power spent to produce the flux of kinetic energy from the pulsed jets ($P_j = (\rho \overline{V_j^3}/2)A_j$, where A_j is the exit jet total area and $(\overline{V_j^3})^{\frac{1}{3}} = 7m/s$ for the HF actuation). For the present configuration (whose drag coefficient is of the order of 0.3 [19] [25]) and considering the HF actuation, the estimated ζ is 16 which indicates a considerable recovery of mechanical power when actuation is performed.

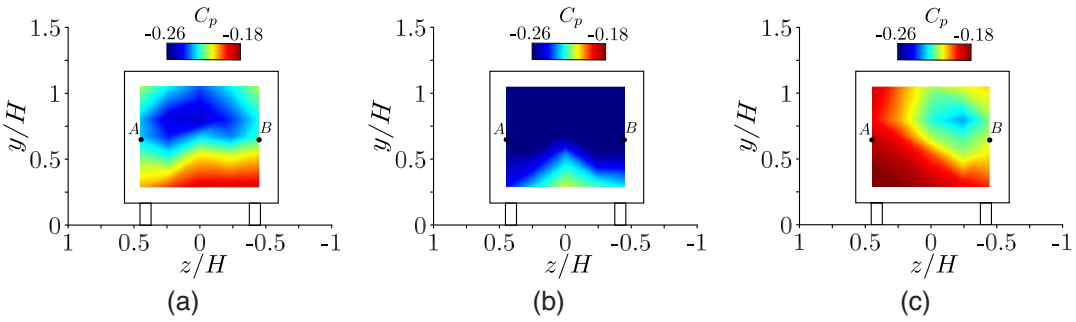

Figure 4. Pressure distribution (C_p) on the rear surface of the model. a) Natural flow. b) LF actuation. c) HF actuation. The pressure is linearly interpolated in the rectangular area colored in the pictures based on the 17 pressure taps installed on the base surface. Points A and B indicated are discussed in the text.

Interestingly, asymmetric and symmetric distributions are noted. Both natural and LF controlled flows have an almost symmetric distribution of pressure contrary to the HF actuated case, having a clear asymmetry. The pressure signals were averaged over 180 seconds for the natural flow and during 45 seconds for the controlled configurations. Recently, Grandemange et al. [15],[22] have observed asymmetries due to long time dynamics in such blunt geometries. They showed the existence of random changes of flow topology, where the wake is oriented in two different directions evidenced by the sign of the pressure gradients on the back part of the model. When they are positive, low-pressure regions are located in $z < 0$ and the wake is asymmetrically directed to the opposite side. Considering the filtered (moving average over windows of 0.5s) evolution of the lateral pressure difference obtained by the difference of two extreme pressure taps (indicated by A and B in the figures), defined by $(\Delta C_p)_z = C_{pA} - C_{pB}$, we observe similar results which are illustrated in figure 5(a,b,c). The probability density functions (PDF) of the differences are also depicted. Above mentioned symmetry properties are verified by two peaks on the PDF curve of the asymmetric HF configuration and just one peak for the LF actuation centered at $(\Delta C_p)_z = 0$, indicating a time-averaged centered wake. For this symmetric pressure distribution in LF forcing, $(\Delta C_p)_z$ reach maximum values of about 0.05, smaller than those observed for

the reference flow and HF forcing (maximum differences of about 0.08).

Grandemange's works remark the high sensitivity of the wake for lateral perturbations: even very small perturbations on the set-up could select one of the two random topologies (right and left directioning of the wake). These reflexive topologies can be mathematically averaged to obtain the statistical symmetric mean flow, which experimentally would corresponds to an infinite time-averaging procedure for a perfectly symmetric set-up. Although the pulsed jets could induce slight asymmetries due to the operation of solenoid valves and the mounting, they are not observed in the LF controlled flow indicating that the wake dynamics for this configuration is strong enough (in the dynamic point of view) to inhibit these changes of topology.

In view of the mentioned changes in the mean pressure and long-time dynamics, we analyze now the near wake velocity field in order to identify correlated changes in the wake flow that could explain these pressure variations.

3.2 Near wake mean velocity and statistics

We consider the effects of periodic control on the near wake. Contour maps of the mean streamwise velocity as well as the streamlines of the projected velocity field on the symmetry plane are presented in figure 6(a,b,c). Considerable reduction of the mean recirculation length for LF actuation is remarked, where the streamwise position of the saddle point (indicated by S in the pictures) is reduced by 27% from x/H= 1.42 to x/H= 1.04 , as indicated in the table 2. This reduction is commonly linked to significant increase of pressure drag in nominally two-dimensional flows [2], [7] indicating a configuration with lower base pressure as measured and commented before. Interestingly, however, HF actuation does not promote considerable changes in the recirculation length but on the vertical (wall-normal) position of the saddle point; this position (y/H) increases from y/H= 0.335 to y/H=0.454 (about 35%) suggesting the existence of a thinner and more symmetric wake whose streamlines are differently oriented when compared to the natural flow.

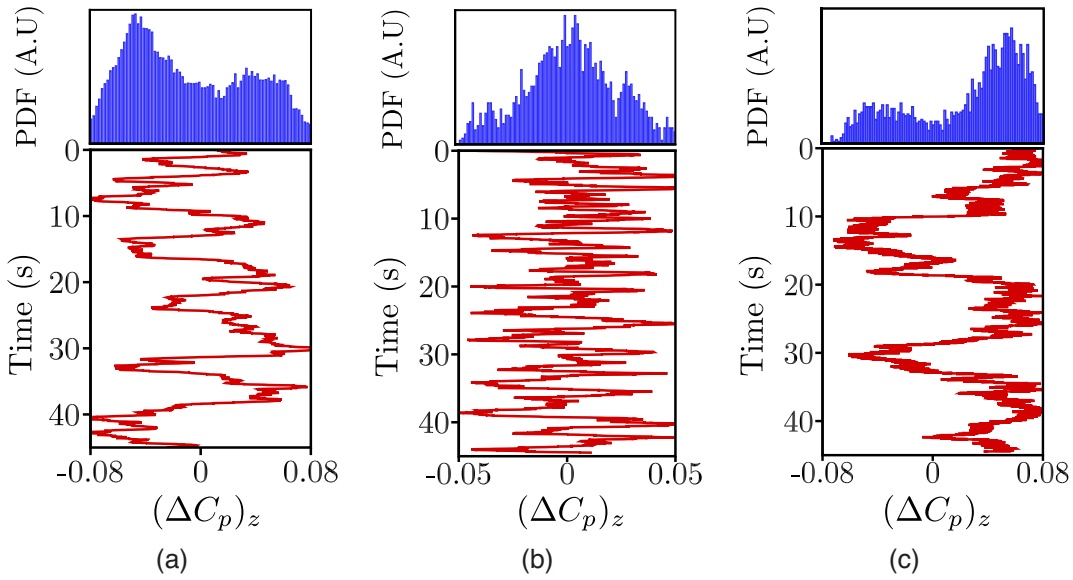

Figure 5. Pressure gradients on the back surface of the Ahmed body and their probability density function (PDF). a) Reference flow. b) LF forcing. c) HF forcing.

Table 2. Mean flow properties

Configuration	**x/H (S)**	**y/H (S)**	**ΔC_p (%)**
Natural flow	1.42	0.335	-
LF actuation	1.04	0.348	-18
HF actuation	1.47	0.454	+10

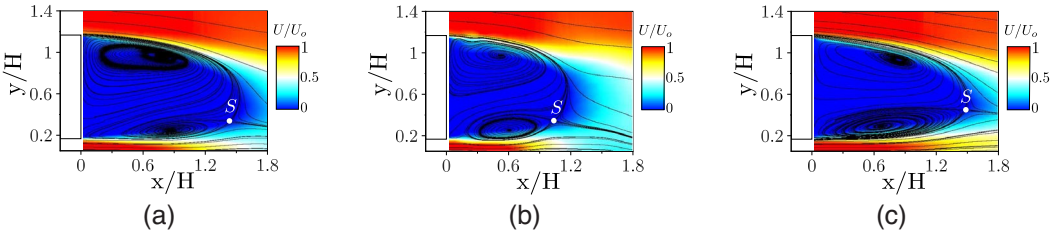

Figure 6. Contour maps of the streamwise velocity and streamlines of the in-plane velocity field on the symmetry plane of the configuration. a) Natural flow. b) LF actuation. c) HF actuation. The point S represents a saddle point of the mean flow at the end of the recirculation region in the wake.

Time-averaged velocity on the transverse (horizontal) plane at mid-height of the model (y/H=0.67) was also measured and analyzed. As the HF flow obtained is asymmetric, we have promoted data symmetrization following [22]. From the time-averaged flow, we perform a reflexion of the lateral and streamwise velocities and calculate a new symmetric mean flow. This would correspond to a mathematically symmetric mean flow which experimentally represents the time-averaged flow for a long time acquisition PIV measurement and a perfectly symmetric set-up. We remark that this procedure is valid only if the random change of topology is really observed, as shown in the present work by the pressure gradients on the rear surface of the model (see last section).

Mean-flow on the horizontal plane is showed in figure 7(a,b,c). The recirculation region for the low frequency actuation is clearly reduced, in the same manner as previously observed in the symmetry plane. Reference flow and HF actuation seem quite similar, despite the important pressure drag reduction measured. We focus now on analyzing differences between the reference flow and HF forcing case in order to analyze the drag reduction mechanisms.

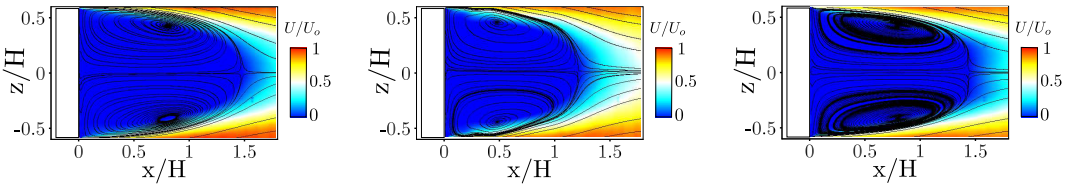

Figure 7. Same as figure 6 in the transverse (horizontal) plane at (y/H=0.67).

The base pressure of a bluff body is the main source of its total pressure drag. This pressure is part of the streamwise momentum balance for a closed surface in the near wake flow, in which the time-averaged pressure and the Reynolds stresses are the main contributors [23]. Mean properties of the recirculation region might be viewed as a key parameter to set the back pressure of the model. The topology of the time-averaged flow, described by the velocity field and its curvature, induces pressure gradients between the outer flow and the wake region due to mean acceleration effects. Besides, the average of the transport of fluctuating streamwise momentum by the fluctuating velocity normal to the surface of the closed surface dictates the mentioned balance in the wake.

In order to quantify the change of mean topology highlighted for the high-frequency actuation and its drag reduction effect, we study the evolution of the projected separating streamlines carefully selected on both planes. These streamlines were manually chosen from a starting point located at y/H=1.16 (upper corner in the symmetry plane), y/H=0.167 (lower corner in the symmetry plane) and z/H=±0.58 (left/right corners on the horizontal plane). The robustness of the results obtained was verified by making a sensitivity analysis to the mean streamline starting point. Figure 8(a,b,c) shows the streamline path and the velocity angles for both natural flow and high-frequency forcing, respectively for the upper, lower and lateral streamlines (depicted in detail in the pictures).

The first striking observation is that the mean separating angle is strongly modified by HF actuation. Initial angles (absolute values) of about 4-8° are measured for the actuated flow, greater than the values for the reference flow where the angles are considerably smaller. Moreover, it is possible to note an interesting change of the angle evolution for both configurations. A plateau-type evolution (from x/H=0.1 to about x/H=0.2) is observed for the HF case indicating smaller angle variations along the time-averaged shear layer development. On the other hand, an almost monotonic dependence on the streamwise position is noted for the natural flow. In the time-averaged point of view, this modification corresponds to a reduction of mean pressure gradients across the mean separating streamlines, inducing larger values of the pressure in the wake region and thus a reduction of the pressure drag.

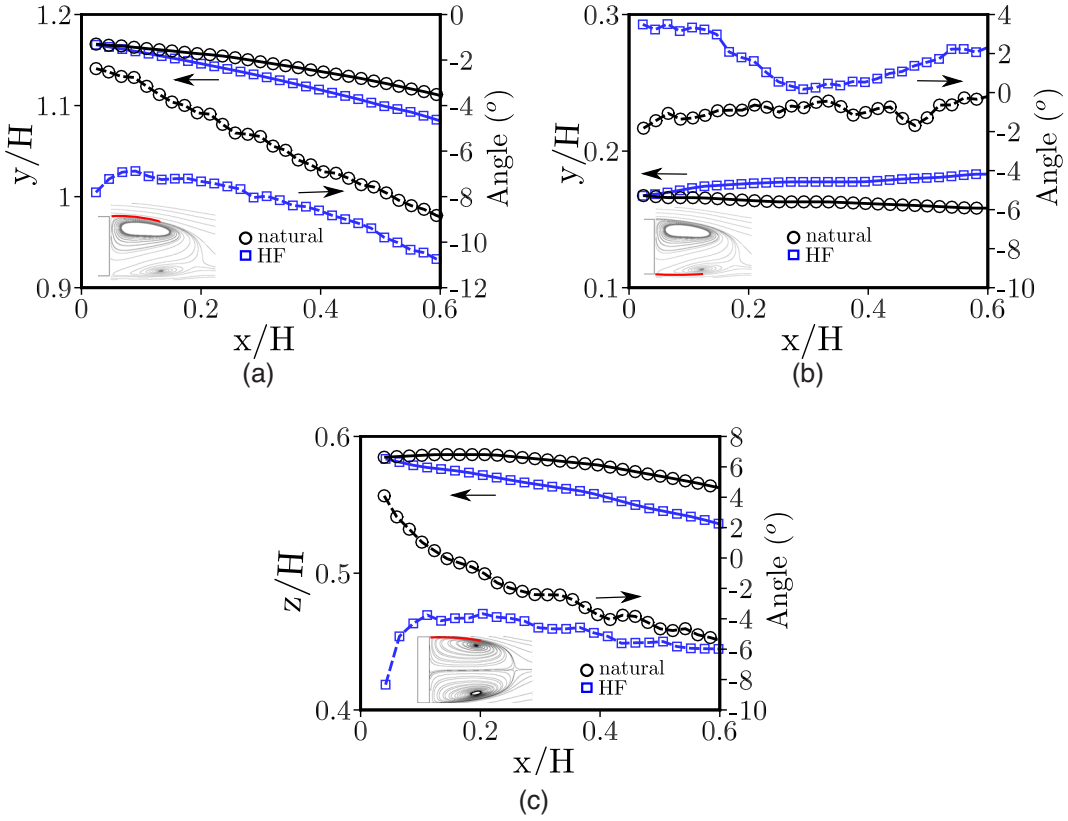

Figure 8. Separating streamlines path (continuous lines) and velocity angle evolution (dashed lines) along the streamwise direction for the natural flow (circles) and HF forcing (squares). The starting point of the streamlines are a) y/H=1.16 (upper streamline), b) y/H=0.167 (lower streamline) and c) z/H=0.58 (lateral streamline). The streamlines are highlighted (in red) in the detailed picture of the mean streamlines.

Finally, one observes, very near to the base of the model, a change in the convexity of the mean separating streamlines in the HF case, particularly clear in figure 8c where the absolute value of the mean angle decreases before the plateau. Therefore, for HF, separating streamlines are convex near the base and concave further away. This again should be associated to important changes of the mean pressure gradients near the back surface of the model. Refined measurements are presently performed and dynamical mechanisms responsible for these observations are under study.

As discussed before, the role of the fluctuating velocities on the mean properties of the recirculation region is of fundamental importance. To get an overview of the global flow dynamics and to characterize these fluctuations in the near wake, we turn our attention to the analysis of the time-averaged Reynolds stresses based on the velocity fluctuations. Figure 9 (a,b,c,d) depicts the distribution of the in-plane turbulent kinetic energy (T_{kin}) defined here as $T_{kin} = (< u'u' > + < v'v' >)/2U_o^2$ (for the

symmetry plane z/H=0) and T_{kin} = (< $u'u'$> + < $w'w'$>)/2U_o^2 (for the horizontal plane y/H=0.67), where u′, v′ and w′ stand for the velocity fluctuations in the Reynolds decomposition.

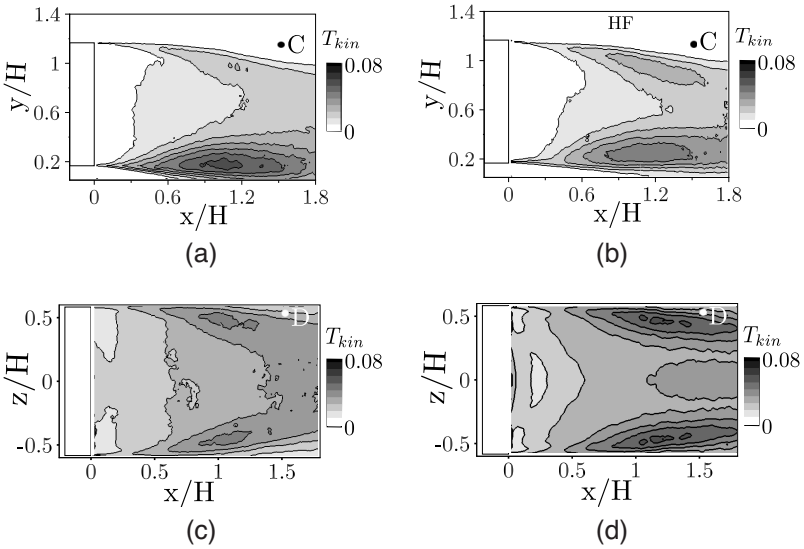

Figure 9. Contour maps of the in-plane turbulent kinetic energy (T_{kin}) in the symmetry plane (a,b) and transverse plane (c,d), respectively for reference flow and HF forcing. Points C and D are described in section 3.3.

In both configurations, this energy is concentrated in the regions of the shear layer development along the wake. Interestingly, in the symmetry plane, the velocity fluctuations are more pronounced on the lower shear layer, indicating a stronger dynamic activity of the underflow in this region.

The effect of the high frequency forcing is a reduction of turbulent kinetic energy in the lower shear layer (compare figures 9(a,b)). An increase of T_{kin} along the upper and lateral shear layers is however clear (see figures 9(a,b) and 9(c,d)). Note that, in the horizontal plane, this evolution is due to an increase of <u′u′> while <w′w′> remains approximately the same in HF pulsed case - corresponding figures are not shown here for brevity.

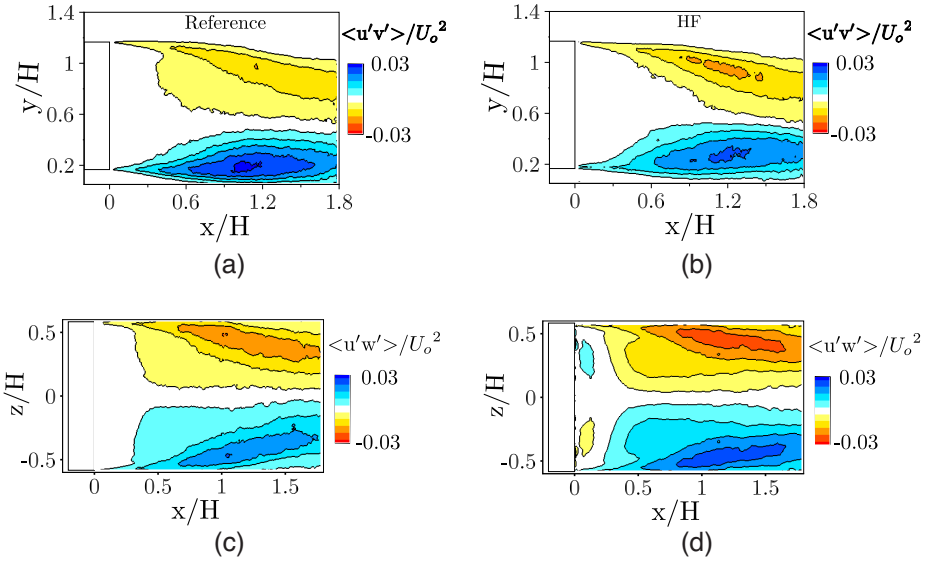

Figure 10. Shear-stresses <u′v′> in the symmetry plane in the wake (a,b) and <u′w′> in the horizontal plane (c,d) respectively for the reference flow and HF forcing.

The mean streamwise momentum balance in the wake depends on the Reynolds shear stresses <u′v′> and <u′w′>. When comparing the reference case to the HF actuation, these quantities decrease along the lower shear layer (see figure 10(a,b)) while an increase is observed in the upper and lateral shear layers (figures 10(c,d)). More precisely, the integral of <u′v′> (respectively <u′w′>) computed along the line of maximum Reynolds shear stress between x/H=0.2 and x/H=1.0 decreases by 19% in the lower shear layer and increases by 8% and 21% in the upper and lateral shear layers respectively.

A complete estimation of the momentum balance terms is not available, of course, using 2D2C PIV in two perpendicular planes for this 3D body. However, from the available measurements, it seems clear that the main contributor to the decrease of drag is due to the modification of the topology of the mean flow and, in particular, to the orientation and curvature of the separating streamlines.

After characterization of the time-averaged flow and the velocity fluctuations on the wake, we study now some basic dynamical aspects of both natural and controlled flow configurations.

3.3 Near wake dynamics

Dynamical aspects of the near wake for the previously analyzed flows will be described by the measurement of instantaneous flow and power spectral density obtained by hot wire anemometry.

We start the analysis by the visualization of representative flow snapshots commonly observed during the time evolution of natural and controlled flows. The velocity magnitude, interpreted here as the norm of the velocity field, is presented in figure 11(a,b,c) respectively for natural, LF and HF flows. It is possible to observe the recirculation region formed by the development of the upper and lower shear layers separated from the trailing edges of the model.

Considerable vortex roll-up is identified for the LF forcing in the lower shear layer region. Such intense roll-up is rarely noted in the reference flow and corresponds to a strong coupling of actuation modes and wake natural frequencies (see also figure 12), as the dimensionless frequency for LF actuation is of the same order of the natural flow modes previously discussed in the section 2.3. It explains the high intensity of velocity fluctuations (not shown in the present work for brevity) in this region and a significant increase of entrainment in the separated shear layer, which seems to be one of the main causes for the important reduction of recirculation length measured in this time-averaged flow [24]. Similar behavior was also noted for the horizontal plane snapshots, where higher dynamical activity was observed in the lateral shear layers.

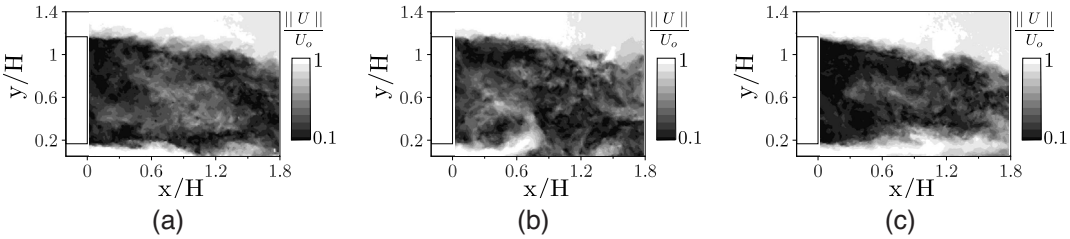

Figure 11. Instantaneous flow (snapshots) of the reference case (a), LF forcing (b) and HF forcing (c). The grey levels corresponds to the magnitude (norm) of the velocity field in the symmetry plane of the configuration.

High-frequency forcing, on the other hand, depicts flow snapshots where a thinner wake is present. Besides, underflow developing from the separated shear layer is less fluctuating and extends its velocity magnitude for longer streamwise positions.

Power spectral density (PSD) is obtained from point velocity measurements acquired by a single hot wire probe. The amplitude of the spectra was normalized using the variance of each velocity signal (resulting in a PSD of dimension 1/Hz). The velocity magnitude was measured at two points at the end of the time-averaged recirculation region, whose coordinates (x/H, y/H, z/H) are given by C(1.5, 1.17, 0) and D(1.5, 0.67, 0.52) (as illustrated in figure 9). These points are localized respectively in the symmetry and horizontal planes of the configuration (PIV planes studied before). Figure 12(a,b) presents the velocity spectra in both points for the natural flow and for the LF/HF actuation.

First, the spectra of the reference flow illustrates two peaks corresponding to St = 0.2 (C) and St = 0.163 (D). These modes were also observed in the recent work of [15] and indicate two global shedding

scales typically observed when the geometry presents two different geometric scales, namely the height (H) and width (W) of the model. These two modes, when respectively non-dimensionalized by both scales, present almost the same dimensionless frequency.

Both actuation do not change considerably the values of these frequencies but mainly their amplitude. LF forcing increases the amplitude of the first mode and introduces in the flow the actuation frequency F_i (St_H =0.4) and its harmonics. The amplitude of the first wake mode (St = 0.2) is greater than of the actuation mode for point (C). A different scenario observed for the second wake mode (St = 0.163) measured in the point (D), where the amplitude of the actuation is greater. Interestingly, a small change of the second wake mode (point D) is observed when LF is applied changing the mode from St = 0.163 to St = 0.18. Besides, St = 0.2 is also detected for this configuration (see dashed lines in figure 12b). High-frequency forcing, however, reduced the amplitude of both modes, particularly observed in point D where the peak of the wake mode is clearly spread to nearby frequencies.

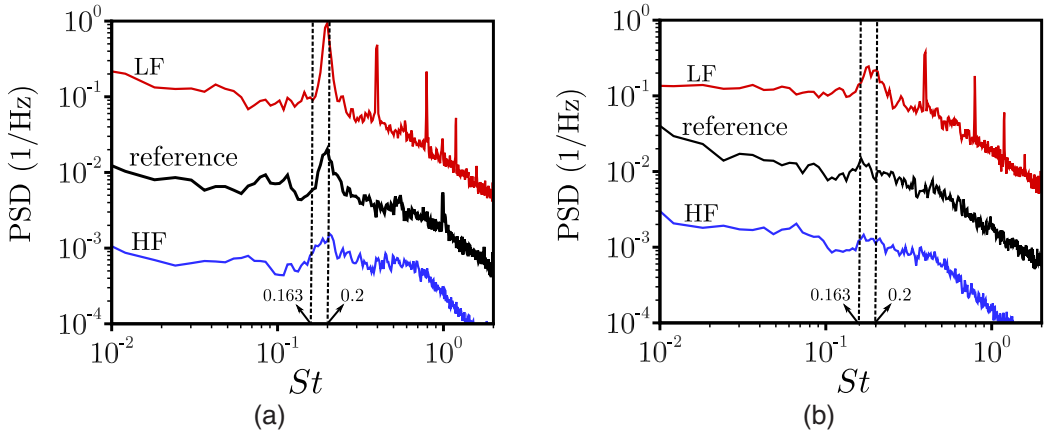

Figure 12: Power spectral density (PSD) of velocity signals in the wake for the reference, LF and HF flows. a) Point C. b) Point D. See text for the description of both points. The dimensionless frequency f is given by $St = H f / U_o$. Each PSD is shifted by one decade for clarity. Vertical dashed lines are located at St = 0.163 and St = 0.2.

4. CONCLUSION

We experimentally reported the capability of periodic pulsed jets to change the rear pressure distribution of a three-dimensional blunt body for a Reynolds number of 3.10^5. The geometry studied here is the square-back Ahmed model. The rear pressure variation is accompanied by important changes of the velocity field in the wake. Two forcing frequencies were studied and their effects on the wake were detailed.

For the lower frequency actuation, a considerable decrease of rear pressure is achieved inducing increase of the total drag of the model. The time-averaged recirculation region is considerably smaller than the reference base flow. The presence of strong vortex roll-up in the lower shear layer was identified which explains the increase of entrainment in the wake reducing then its recirculation length. Besides, velocity spectra for this configuration illustrated amplification of the main modes commonly observed in the wake of this geometry. Pressure gradients on the rear surface showed the disappearance of the bi-modal behavior recently described in the literature.

When the actuation frequency is higher, considerable recovery of the model's base pressure was obtained, where the pressure drag reduces by 10% and the estimated total drag reduction is about 7%. This actuated flow presented damped velocity fluctuations on the lower part of the wake (lower shear layer) and indicates a narrower and more symmetric time-averaged wake. A deviation of the mean separating streamlines is clearly observed. This global deviation of the wake flow was correlated to changes of the pressure gradients near the model's base and then to the pressure drag reduction. The power spectral density of velocity shows that the global wake modes are damped in this case.

The separated shear-layers of blunt bodies corresponds to the first step for the formation of a recirculation region and their development is crucial to the whole characteristics of the wake namely

its time-averaged topology and dynamics. Actuation in this very sensitive region may be a remarkable candidate in order to achieve base pressure modifications whose direct effect is linked to drag control, which here is exemplified by the use of active pulsed jets.

The present study shows that pulsed jets blown tangentially to the base flow shear layer trigger different physical mechanisms according to the control parameters. LF pulsing enhances the global wake mode activity and leads to an increase of drag. On the contrary, dynamical effects associated to the particular flow control strategy provide a significant drag decrease at HF forcing. Systematic variation of Reynolds number and control parameters are presently on their way.

5. ACKNOWLEDGMENTS

The thesis of D.B is supported financially by PSA - Peugeot Citroën and ANRT in the context of the OpenLab Fluidics between PSA and Institute Pprime. The authors acknowledge the funding of the Chair of Excellence - Closed-loop control of turbulent shear flows using reduced-order models (TUCOROM)-supported by the French Agence Nationale de la Recherche (ANR). The authors warmly acknowledge the support during the experiments by J.M. Breux, J.C. Boueilh, G. Pujals and Y.Goraguer and fruitful discussions with A. Spohn and J. Pfeiffer.

REFERENCES

[1] A. Roshko. On the drag and shedding frequency of two dimensional bluff bodies. *NACA Technical Note*, NACA TN 3169, 1954.

[2] A. Roshko. Perspectives on bluff body aerodynamics. *J. Wind Eng. Ind. Aerodynamics*, 49:79–100, 1993.

[3] S. R. Ahmed, G. Ramn, and G. Faltin. Some salient features of the time averaged ground vehicle wake. *SAE Tech. Report. No. 840300, Society of Automotive Engineers, Inc.*, Warrendale, PA, 1984.

[4] T. Morel. The effect of base slant on the flow pattern and drag of three-dimensional bodies. In G. Sovran, T. Morel, and W. T. Mason Jr., editors, *Aerodynamic Drag Mechanisms of Bluff Bodies and Road Vehicles*. Plenum Press, New York - London, 1978.

[5] H. Choi, J. Lee, and H. Park. Aerodynamics of heavy vehicles. *Ann. Rev. Fluid. Mech.*, 46:441–468, 2014. 17

[6] H. Choi, W.P. Jeon, and J. Kim. Control of flow over a bluff body. *Ann. Rev. Fluid. Mech.*, 40:113–139, 2008.

[7] M. Pastoor, L. Henning, B. R. Noack, R. King, and G. Tadmor. Feedback shear layer control for bluff body drag reduction. *J. Fluid Mech.*, 608:161–196, 2008.

[8] V. Parezanovic and O. Cadot. Experimental sensitivity analysis of the global properties of a two-dimensional turbulent wake. *J. Fluid Mech.*, 693:115–149, 2012.

[9] D. J. Parkin, M. C. Thompson, and J. Sheridan. Numerical analysis of bluff body wakes under periodic open-loop control. *J. Fluid Mech.*, 739:94–123, 2014.

[10] B. Khalighi, S. Zhang, C. Koromilas, S. R. Balkanyi, L. P. Bernal, G. Iaccarino, and P. Moin. Experimental and computational study of unsteady wake flow behind a bluff body with a drag reduction device. *SAE paper*, 2001.

[11] B. Khalighi, K. H. Chen, and G. Iaccarino. Unsteady aerodynamic flow investigation around a simplified square-back road vehicle with drag reduction devices. *J. Fluids Engng.,* 134 (6):16 pages, 2012.

[12] R. Littlewood and M. Passmore. The optimization of roof trailing edge geometry of a simple square-back. *SAE paper 2010-01-0510*, pages 151–160, 2010.

[13] M. Roumeas, P. Gillieron, and A. Kourta. Analysis and control of the near-wake flow over a square-back geometry. *Compt. and Fluids*, 38 (1):60–70, 2009.

[14] E. Wassen, S. Eichinger, and F. Thiele. Simulation of active drag reduction for a square-back vehicle. In R. King, editor, *Active Flow Control II, NNFM*, pages 241–255. Springer-Verlag, Berlin, 2010.

[15] M. Grandemange, M. Gohlke, and O. Cadot. Turbulent wake past a three-dimensional blunt body. part 1. global modes and bi-stability. *J. Fluid Mech.*, 722:51–84, 2013.

[16] P. Joseph, X. Amandolese, and J. L. Aider. Drag reduction of the 25 slant angle ahmed reference body using pulsed jets. *Exp. Fluids*, 52:1169–1185, 2012.

[17] P. Gillieron and A. Kourta. Aerodynamics drag control by pulsed jets on simplified car geometry. *Exp. Fluids*, 54:16 pages, 2013.

[18] A. Oxlade and J. F. Morrison. Open-loop control of an axisymmetric turbulent wake using high frequency periodic jet blowing. *ETC - 14*, Lyon, France., 2013.

[19] S. Krajnovic and L. Davidson. Numerical study of the flow around a bus-shapped body. *J. Fluids Engng*., 125:500–509, 2003.

[20] M. Grandemange, A. Mary, M. Gohlke, and O. Cadot. Effect on drag of the flow orientation at the base separation of a simplified blunt road vehicle. *Exp. Fluids*, 54:10 pages, 2013.

[21] C. M. Ho and P. Huerre. Perturbed free shear layers. *Ann. Rev. Fluid. Mech*., 16:365–422, 1984.

[22] M. Grandemange, V. Parezanovic, M. Gohlke, and O. Cadot. On experimental sensitivity analysis of the turbulent wake from an axisymmetric blunt trailing edge. *Phys. Fluids*, 24, 2012.

[23] S. Balachandar, R. Mittal, and F. M. Najjar. Properties of the mean recirculation region in the wakes of two-dimensional bluff bodies. *J. Fluid Mech*., 351:167–199, 1997.

[24] J. H. Gerrard. The mechanics of the formation region of vortices behind bluff bodies. *J. Fluid Mech*., 25:401–413, 1966.

[25] A. Lahaye, A. Leroy, and A. Kourta. Aerodynamics characterisation of a square back bluff body flow. *Int. J. Aerodynamics*, 4:43–60, 2014.